JMEPEG (2019) 28:1030–1039
https://doi.org/10.1007/s11665-018-3847-z

1059-9495/$19.00

Corrosion Mechanism and Applicability Assessment of N80 and 9Cr Steels in CO_2 Auxiliary Steam Drive

Baojun Dong, Dezhi Zeng, Zhiming Yu, Lele Cai, Shanzhi Shi, Huiyong Yu, Haiyan Zhao, and Gang Tian

(Submitted March 16, 2018; in revised form December 6, 2018; published online January 3, 2019)

Corrosion tests were conducted in a high-temperature high-pressure (HTHP) autoclave to simulate the conditions of CO_2 auxiliary steam drive in gas injection wells. Weight loss tests were performed with the sheets of N80 and 9Cr steels under the testing conditions. The morphology and composition of corrosion products were explored by SEM, EDS, XRD and XPS. The corrosion resistance of 9Cr steel was better than that of N80 steel under the testing conditions. The corrosion rates of N80 and 9Cr met the application requirements in CO_2 auxiliary steam drive. The results broke the constraint in ISO-15156 standards. The corrosion process of N80 steel was mainly affected by the flow velocity. However, the corrosion process of 9Cr steel was mainly affected by temperature. The corrosion resistance of 9Cr steel depended on the $FeCO_3$ content of Cr-rich layer, which was closely related to temperature. The low flow velocity influenced the diffusion process of N80 steel corrosive ions, whereas the high flow velocity influenced the integrity of corrosion scales. Considering the influence of flow velocity on the corrosion of tubing and casing, in the gas injection well, 9Cr steel and N80 steel were, respectively, selected as the materials of tubing and casing.

Keywords CO_2 auxiliary steam drive, CO_2 corrosion, N80 steel, 9Cr steel, temperature, flow velocity

1. Introduction

CO_2 auxiliary steam drive is a new technology to improve the recovery performance of heavy oil reservoir in recent years and shows a good application prospect in oil recovery (Ref 1, 2). Heavy oil viscosity can be reduced through injecting steam and a small amount of CO_2 into heavy oil reservoir. However, during steam injection, the wellbore temperature (160-20 °C) of gas injection wells is high and injected CO_2 will cool the wellbore to generate the water film on the inner wall of wellbore. When steam injection stops, the temperature of wellbore gradually decreases and the water film is formed on the inner wall of wellbore. When CO_2 is dissolved in water, it will form carbonic acid. Carbonic acid will significantly increase the corrosion rate of tubing and casing steel and cause serious corrosion (Ref 3-6). Therefore, a reasonable choice of tubing and casing steels is the key to ensure the safe implementation of CO_2 auxiliary steam drive.

According to the study results of the Kawasaki Heavy Industries and Sumitomo Metal Industries, when the temperature was higher than 180 °C, stainless steel (22Cr and 25Cr steel) containing the higher level of Cr should be adopted (Ref 7). However, the expensive 22Cr and 25Cr steel significantly increased the exploitation cost of heavy oil reservoir. The commonly used tube and case steels are much cheaper than recommended steel (22Cr and 25Cr steel), but the applicability of the common tube and case steels in the injection well should be further explored.

The tube and case often serve in complex environments involving multiple corrosion factors, such as temperature, CO_2 partial pressure, and flow velocity (Ref 8, 9). The failure probability of tube and case was higher in the complex environment of corrosion factors. Zhu et al. reported that the deposition rate of $FeCO_3$ increased with the increase in temperature (Ref 10). Gao et al. found that as the temperature increased, the corrosion scales of N80 steel were changed from a membrane structure into a two-layer structure (Ref 11). Zhang et al. observed that the increase in CO_2 partial pressure resulted in the decreased pH value of the solution and the serious corrosion of steels (Ref 12). Guo et al. studied that the corrosion rate of 3Cr steel under the flowing conditions was higher than that under static conditions (Ref 13). Xu et al. reported that the CO_2 partial pressure affected the corrosion morphology of Cr-containing steel through changing the solution pH (Ref 14). Temperature, CO_2 partial pressure, and flow rate had the significant influences on the structure and composition of corrosion products (Ref 15-17). Previous studies focused on the influences of individual factors on the corrosion mechanisms. However, the corrosion failure of tubes and cases is the consequence of multiple factors and it is difficult to determine the main factors affecting the corrosion of tube and case steels based on previous studies. Therefore, it is necessary to determine the main factors affecting the corrosion for developing proper protective measures in gas injection wells.

Moreover, previous studies on the simulated environment of CO_2 corrosion mainly involved the environment of liquid, gas or gas–liquid, which was significantly different from the corrosion environment of high-temperature steam containing CO_2 (Ref 18-20). In CO_2 auxiliary steam drive, gas injection temperature should be controlled within the range of 160-

Baojun Dong, Dezhi Zeng, Zhiming Yu, and **Lele Cai**, State Key Laboratory of Oil and Gas Reservoir Geology and Exploration, Southwest Petroleum University, Chengdu 610500, China; **Shanzhi Shi, Huiyong Yu, Haiyan Zhao,** and **Gang Tian**, Engineering Technology Research Institute of Xinjiang Oilfield Company, Karamay 834000, China. Contact e-mail: zengdezhiswpu@163.com.

220 °C and CO_2 pressure should be controlled within the range of 1-5 MPa. The main corrosion media in the gas injection wells involve high-temperature steam and CO_2. However, the corrosion mechanism of steels in the environment involving high-temperature steam and CO_2 was seldom reported.

The study aims to explore the corrosion behaviors of common tube and case steels in high-temperature steam environment through testing the corrosion behaviors of tube and case steels in simulated CO_2 auxiliary steam drive environment in the high-temperature and high-pressure (HTHP) autoclave. This study explored the main factors affecting the corrosion in gas injection wells as well as the corrosion mechanism of steel in high-temperature steam environment. In addition, a new method for selecting the tube and case steels in gas injection wells was established.

2. Materials and Experiments

2.1 Specimen Preparation

The commonly used tube and case steels include N80 and 9Cr steels. The composition of steels is shown in Table 1. According to the metallographic structures of N80 and 9Cr steels (Fig. 1), the N80 and 9Cr steels microscopically belong to the tempered sorbate and martensite, respectively.

2.2 Weight Loss Test

2.2.1 Testing Scheme. Based on the statistics data of gas injection wells, the main influencing factors of corrosion were determined. The effects of temperature, CO_2 pressure and flow velocity on the corrosion behaviors of steel were studied in the experiment. The experimental scheme is provided in Table 2.

2.2.2 Experimental Methods. According to the ASTM standards, all specimens were machined into a size of 30 × 15 × 3 mm, and each material had 4 parallel specimens in each group. Prior to the test, the specimens were abraded with silicon carbide paper (300-mesh, 600-mesh, 800-mesh, and 1200-mesh) to eliminate scratches, rinsed with distilled water, degreased with acetone, and finally dried with cold air.

Prior to the test, deionized water was pre-oxidized with pure N_2 for 8 h. The each parallel specimen was mounted on specimen holders. The specimen holders were placed in self-designed high-temperature (HT) autoclave (Fig. 2). The volume of high-temperature autoclave was 4 L. Deionized water (60 mL) was poured into the autoclave. The specimen was in the steam environment. Before the autoclave was sealed, the autoclave was deoxygenated with pure N_2 gas for 3 h. When the autoclave was sealed, N_2 was purged into the autoclave for 30 min to remove air. After the autoclave was heated to the experimental temperature, CO_2 gas was injected into the autoclave and the flow velocity was then set for the test. After the test, the four parallel specimens of each group were taken out. After each corrosion test, the specimens were rinsed with deionized water, dehydrated with alcohol and dried in the air. Three specimens were, respectively, descaled in the solution (100 mL of 1.19 g/mL hydrochloric acid +1000 mL of deionized water + 10 g hexamethylene tetramine), rinsed with distilled water, dehydrated with alcohol and then dried in air. The another specimen was used to analyze the morphology and composition of corrosion products.

Before and after the tests, the specimen was weighed in an electronic balance with a precision of 0.1 mg and then stored in a desiccator. The corrosion rate is calculated as (Ref 11, 21):

$$v = 87600\frac{\Delta m}{\rho A \Delta t}, \quad \text{(Eq 1)}$$

where v is corrosion rate (mm/a); Δm is the weight loss (g); ρ is the density of steel (g/cm^3); A is the surface area (cm^2); Δt is the corrosion time (h).

2.3 Morphological Observation and Composition Analysis

The corrosion scales were characterized by scanning electron microcopy (JSM-7500F). The corrosion products on the corroded specimens were analyzed by using x-ray diffraction (XPert Pro MPD) and XPS (Phi-Quantera II).

3. Results and Discussion

3.1 Corrosion Rate

Figure 3 shows the average corrosion rate of steels under various testing conditions. The average corrosion rate of the steels was the average of three specimens. As shown in Fig. 3, the corrosion rate of N80 steel is higher than that of 9Cr steel. Compared with N80 steel, 9Cr steel showed the better corrosion resistance under experimental conditions.

3.1.1 Macroscopic Appearance of Corrosion Scales. The macroscopic morphologies of N80 and 9Cr steels under the maximum corrosion rate are shown in Fig. 4. As exhibited in Fig. 4a, corrosion products of N80 steel are black. In Fig. 4b, the corrosion of 9Cr was slight and corrosion products of 9Cr steel are blue.

3.1.2 SEM Observation and EDS Analysis of Corrosion Products. Figure 5 shows the surface morphology and corresponding EDS results of 9Cr steel at various temperatures. The corrosion films of specimen were complete and dense (Fig. 5A). The main elements in the corrosion products of 9Cr steel were Fe, C, Cr and O (Fig. 5B). The Cr content in the 9Cr steel corrosion products was higher than that in the matrix, indicating that Cr enrichment occurred on the surface of the specimen. The crystals of corrosion products on the surface of the specimen were cubic, and the crystal size was 1-1.5 μm (Fig. 5C). The Cr content in the area (marked with a in Fig. 5A) was slightly higher than that in the matrix (Fig. 5E). Round crystals were scattered on the surface of the specimen,

Table 1 Chemical compositions of steels (wt.%)

Steel	C	Si	Mn	P	S	Cr	Mo	Ni	Nb	Ti	Fe
N80	0.24	0.22	1.19	0.013	0.004	0.036	0.021	0.028	–	–	Bal.
9Cr	0.10	0.12	0.46	–	–	9.30	–	–	–	0.06	Bal.

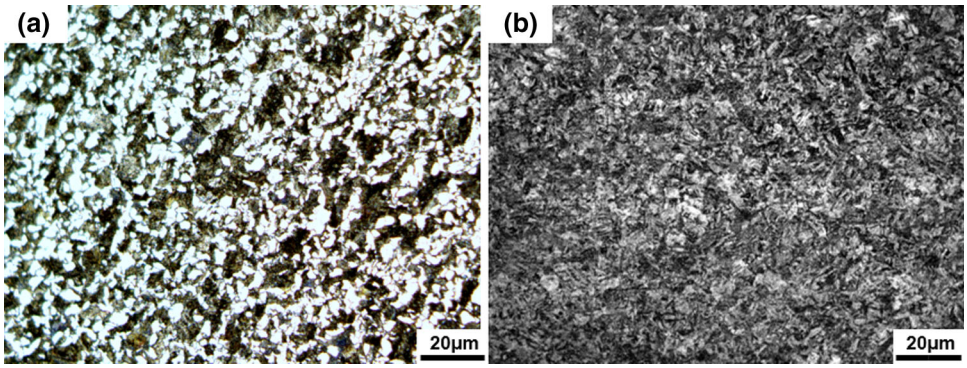

Fig. 1 Metallographic structures of steels (a: N80; b: 9Cr)

Table 2 Testing conditions

Materials	Influencing factors	Temperature, °C	CO_2 pressure, MPa	Flow velocity, m/s	Test time, h
N80	Temperature	160	2	Static	72 h
9Cr		180	2	Static	72 h
		200	2	Static	72 h
		220	2	Static	72 h
	CO_2 pressure	160	1	Static	72 h
		160	2	Static	72 h
		160	3	Static	72 h
		160	4	Static	72 h
	Flow velocity	160	2	3	72 h
		160	2	4.5	72 h
		160	2	6	72 h

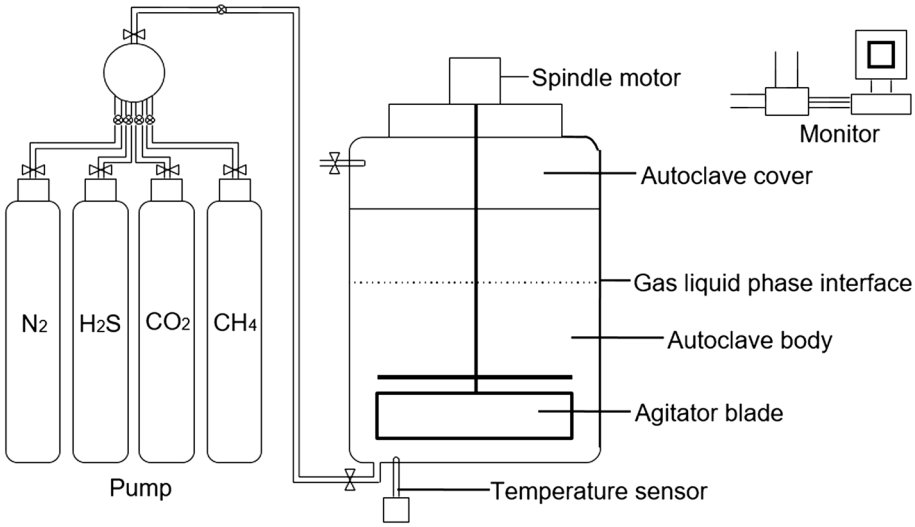

Fig. 2 Schematic diagram of dynamic HT autoclave

and the size of crystals was below 1 μm (Fig. 4f). Scaly corrosion products completely covered the metal matrix (Fig. 5I). Some corrosion products were mixed together. The Cr content in corrosion products was much lower than that in the matrix (Fig. 5J).

Figure 6 shows the surface morphology and corresponding EDS results of N80 steel under various flow velocities. Cubic corrosion crystals were deposited on the surface of the specimen to form uneven corrosion scales. Corrosion scales peeled off, and a circular hole was formed in a local area (Fig. 6B). There were many holes on the surface of corrosion products (Fig. 6C). The main elements in the N80 steel corrosion products were Fe, C, Cr and O (Fig. 6D–F).

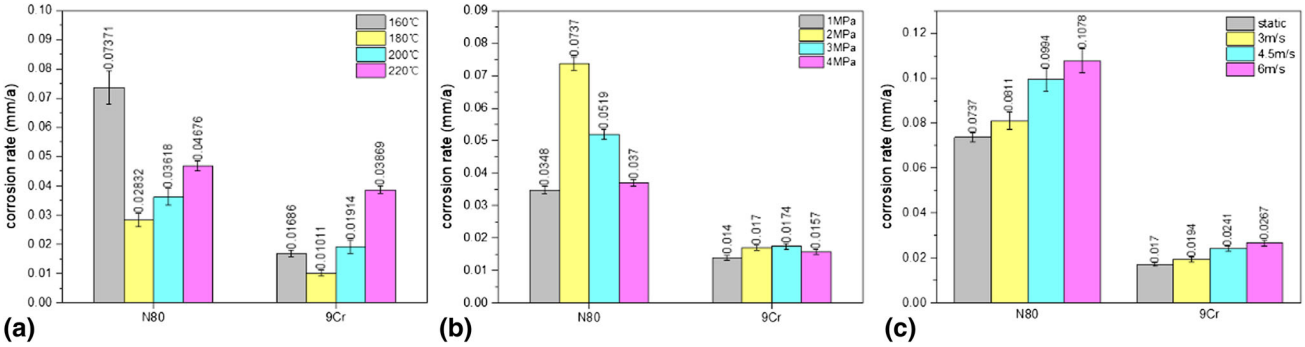

Fig. 3 Average corrosion rate of steel under different testing conditions (a: T: 160-220 °C, P_{CO2}: 2 MPa, f: static; b: T: 160 °C, P_{CO2}: 1-4 MPa, f: static; c: T: 160 °C, P_{CO2}: 2 MPa, f: 0-6 m/s)

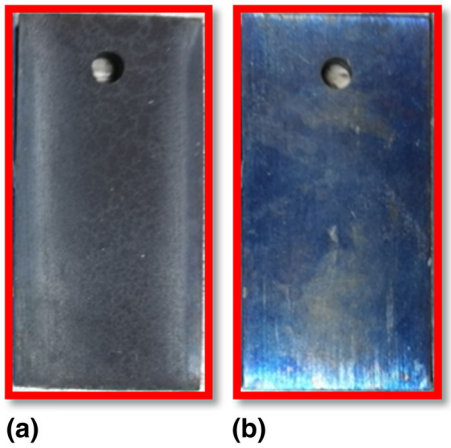

Fig. 4 Macroscopic morphologies of steels (a: N80 steel, T: 160 °C, P_{CO2}: 2 MPa, f: 6 m/s; b: 9Cr steel, T: 220 °C, P_{CO2}: 2 MPa)

3.1.3 XRD and XPS Analysis of Corrosion Scales. The XRD results of N80 and 9Cr steels under the maximum corrosion rate are shown in the Fig. 7. Fe_2O_3 and Fe could be detected (Fig. 7a). The result was consistent with the XPS results. Only 3 peaks were observed and determined as Fe peak through the jade analysis (Fig. 7b).

The corrosion product film of 9Cr was thin, so it was difficult to analyze the composition of corrosion products with XRD. To further study the corrosion products, the XPS was used to analyze to the elemental composition. Figure 8 shows the XPS results of 9Cr steel under static conditions (160 °C and 2 MPa CO_2). The C 1s peaks at 283.6 eV and 284.6 eV corresponded to adventitious carbon (Fig. 8a). The Cr $2p_{3/2}$ peaks at 577.1 eV was ascribed to $Cr(OH)_3$ and Cr_2O_3 (Fig. 8b). The $Fe2p_{1/2}$ peaks at 710.7 eV and $Fe2p_{3/2}$ peaks at 724.4 eV could be ascribed to $FeCO_3$ or Fe_2O_3 (Fig. 8c). The O1s peaks at 530.8 eV and 531.4 eV corresponded to $FeCO_3$, Fe_2O_3, $Cr(OH)_3$ and Cr_2O_3 (Fig. 8d). The XPS analysis results indicated that the corrosion products were $FeCO_3$, Fe_2O_3, $Cr(OH)_3$ and Cr_2O_3 (Ref 22).

In the XPS results of 9Cr steel, a small quantity of Fe_2O_3 and Cr_2O_3 appeared on the surface of 9Cr steel (Fig. 8). $FeCO_3$ was resolved at the high temperature (Eq 2). The specimens were taken out from the autoclave and FeO of corrosion scales was oxidized in air to form Fe_2O_3 (Eq 3) (Ref 22). $Cr(OH)_3$ was dehydrated in air to form Cr_2O_3 (Eq 4) (Ref 23, 24).

$$FeCO_3 \rightarrow FeO + CO_2 \quad \text{(Eq 2)}$$

$$4FeO + O_2 \rightarrow 2Fe_2O_3 \quad \text{(Eq 3)}$$

$$2Cr(OH)_3 \rightarrow Cr_2O_3 + 2H_2O \quad \text{(Eq 4)}$$

Figure 9 shows XPS results of N80 steel after corrosion at 160 °C under 2 MPa CO_2 at 6 m/s. The C1s peak only appears at 284.6 eV, corresponding to adventitious carbon (Fig. 9a). The Fe $2p_{3/2}$ peaks at 724.4 eV corresponded to $FeCO_3$ (Fig. 9b). As for Fe $2p_{1/2}$, the peaks at 710.2 eV could be assigned to $FeCO_3$ (Fig. 9b). The peaks of O1s at 530.6 and 531.9 eV were associated with oxygen in $FeCO_3$ and Fe_2O_3 (Fig. 9c). The XPS analysis results indicated that the corrosion products were $FeCO_3$ and Fe_2O_3 (Ref 22).

4. Discussion

4.1 Analysis of Corrosion Factors

During the process of CO_2 auxiliary steam drive, the corrosion of oil tube and casing tube was mainly affected by temperature, CO_2 pressure, and flow velocity. To quantitatively analyze the influences of temperature, CO_2 pressure, and flow velocity on the corrosion rate, the influencing rate of a corrosion factor is defined as follows:

$$\varphi_i = \frac{v_{i,\max}}{v_{t,\max} + v_{p,\max} + v_{f,\max}}, \quad \text{(Eq 5)}$$

where φ_i is the influencing rate of a corrosion factor; $v_{i,\max}$ is the maximum corrosion rate of a material under a certain testing condition; $v_{i,\max}$ is the maximum corrosion rate of a material at different temperatures; $v_{p,\max}$ is the maximum corrosion rate of a material under different CO_2 pressures; $v_{f,\max}$ is the maximum corrosion rate of a material under different flow velocities.

Figure 10 shows the corrosion factor index of the steels under different testing conditions. The main control factor in the corrosion of N80 steel is flow velocity (Fig. 10a). The main control factor in the corrosion of 9Cr steel is temperature (Fig. 10b). The influences of corrosion factors on oil casing tube should be considered in the selection of materials.

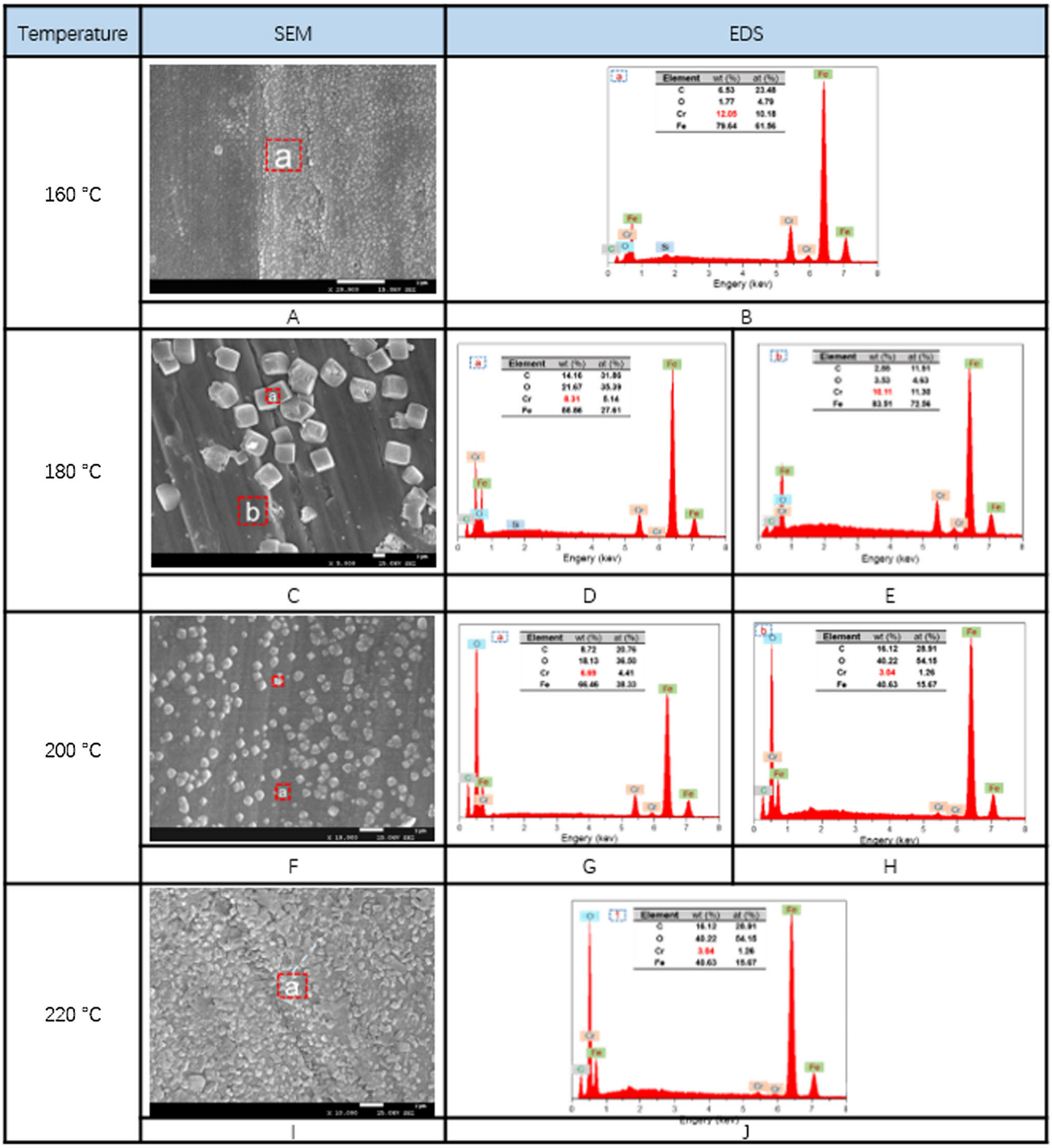

Fig. 5 Surface morphology and element analysis of 9Cr steel at various temperatures

4.2 Corrosion Mechanism

4.2.1 Effects of Temperature on Water Film. During the corrosion process of steel in high-temperature steam containing CO_2, H_2O molecules are firstly absorbed on the surface of specimens to form a thin water film (Fig. 11a). The amount of water-film adsorption is closely related to temperature. Generally, the adsorption of H_2O molecules on steel surface corresponds to a heat release process. The temperature rise is harmful to the adsorption process of H_2O molecules on steel surface. Therefore, the elevated temperature is also not conducive to the formation of water film on steel surface.

4.2.2 Effects of Temperature on the Structure of Cr-Rich Films. In a CO_2 environment, Cr-rich films are formed on the surface of Cr-containing steel. Cr-rich films are mainly composed of a small amount of amorphous $FeCO_3$ and

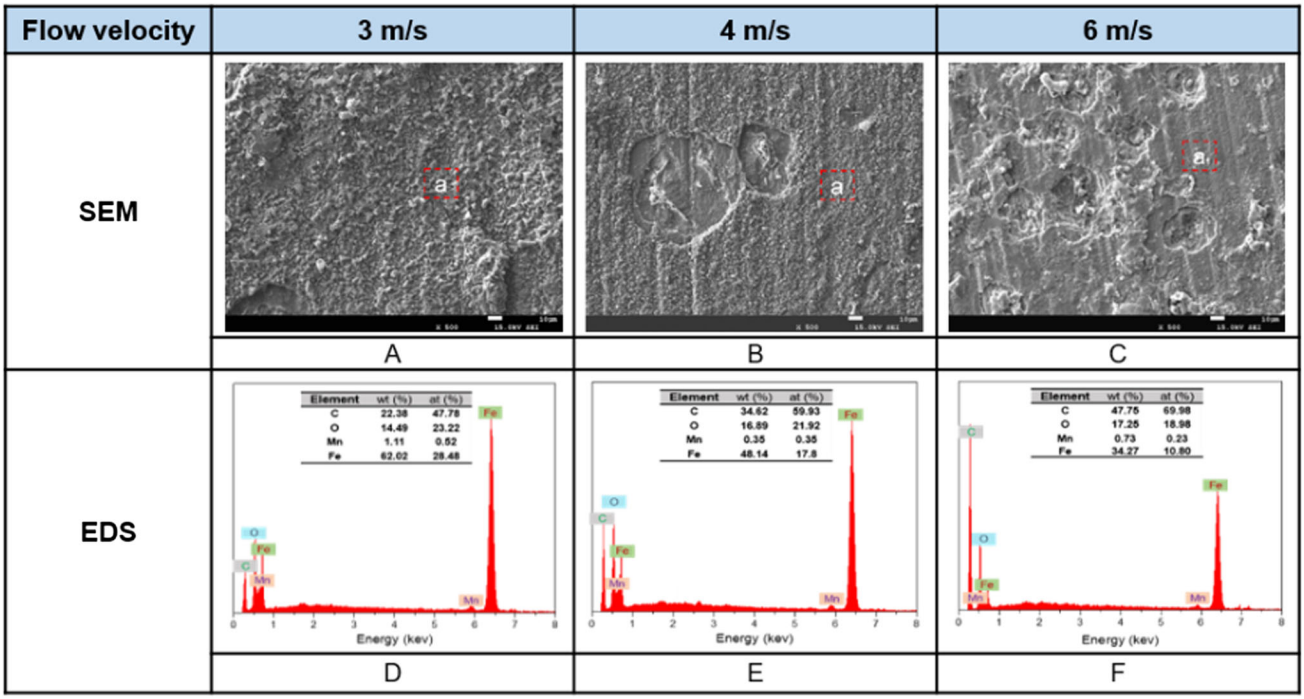

Fig. 6 Surface morphology and element analysis of N80 steel under various flow velocities

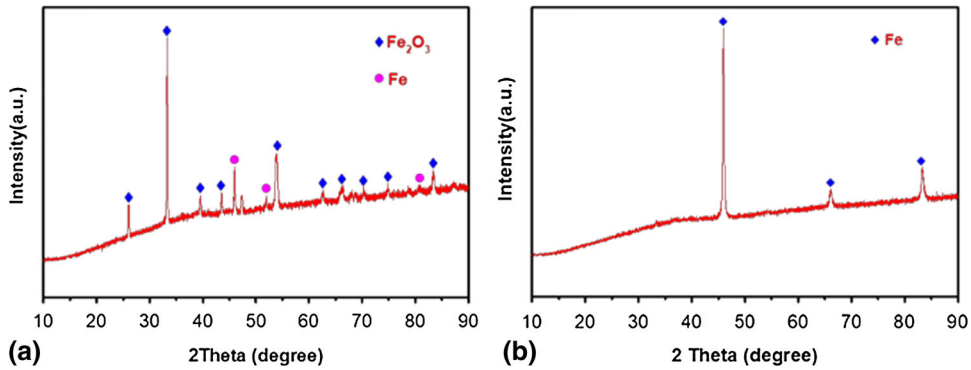

Fig. 7 XRD spectra of corrosion scales on steels (a: N80 steel, T: 160 °C, P_{CO2}: 2 MPa f: 6 m/s; b: 9Cr steel, T: 220 °C, P_{CO2}: 2 MPa)

$Cr(OH)_3$ generated in the hydrolysis of Cr^{3+} (Fig. 11c). The hydrolysis reaction of Cr^{3+} is an endothermic reaction, so the temperature rise can accelerate the hydrolysis of Cr^{3+} (Ref 25, 26). The hydrolysis reaction of Cr^{3+} also produces more H^+ ions, thus causing the rapid decrease in the pH value of the water film (Ref 27, 28). The pH value of the water film determines the growth and nucleation processes of $FeCO_3$ crystals (Ref 29, 30). More $FeCO_3$ crystals are generated at low pH. Therefore, a large number of $FeCO_3$ crystals also accumulate on the Cr-rich layer in the high-temperature environment (Fig. 11d).

4.2.3 Effects of Fluid Flow on the Corrosion Scales. The flow velocity of **a** fluid determines corrosion scales. At a low flow velocity, the fluid promotes the mass transfer process of corrosive ions (Ref 31, 32). Corrosive ions (H^+, HCO_3^- and CO_3^{2-}) rapidly diffuse to the electrode surface and Fe^{2+} quickly leaves from the metal surface. Fe^{2+} ions react with corrosive ions to form the dense $FeCO_3$ layer (Fig. 12b). At a high flow velocity, the wall shearing stress of fluid increases. The combination between the $FeCO_3$ corrosion scales and the metal matrix is weak, so corrosion scales on the surface easily peel off (Fig. 12c).

4.3 Selection of the Materials of Oil Casing Tube

To further study the safe service conditions of gas injection well, the corrosion safety factor of the materials is defined as:

$$\Phi = \frac{0.076}{v_{i,\max}}, \qquad \text{(Eq 6)}$$

where Φ is corrosion safety factor; 0.076 is the corrosion safety control value; $v_{i,\max}$ is the maximum corrosion rate of a material under a certain testing condition. The corrosion safety factor of materials was the ratio of corrosion control index to material corrosion rate. The corrosion safety factor value of a material was higher than 1, indicating that the material was in the safe service state. If the value of the corrosion safety factor of a material was less than 1, the material was in a dangerous service state.

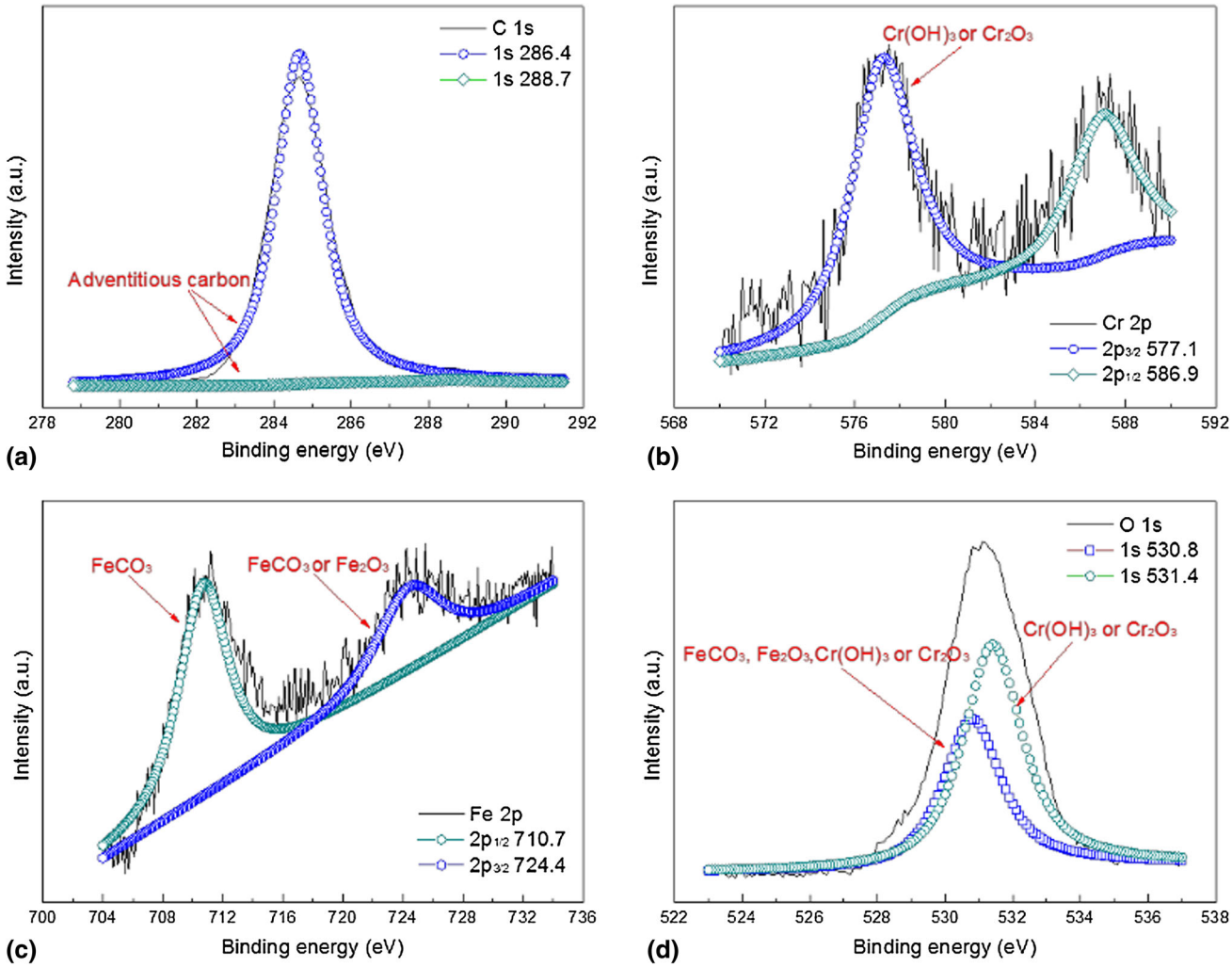

Fig. 8 XPS of 9Cr steel after corrosion under static conditions (160 °C and 2 MPa CO_2): (a) C, (b) Cr, (c) Fe, and (d) O

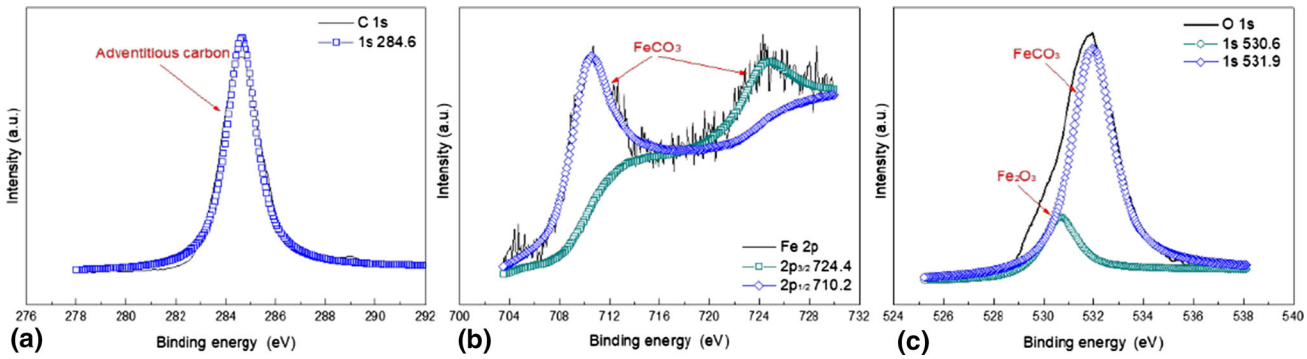

Fig. 9 XPS of N80 steel after corrosion at 160 °C under 2 MPa CO_2 at 6 m/s: (a) C, (b) Fe, and (c) O

Figure 12 shows the corrosion safety factors of steels under different testing conditions. Under different testing conditions, 9Cr steel was in safe service state, whereas N80 steel was in a dangerous service state under different current conditions. During the CO_2 auxiliary steam drive, the steam and CO_2 were injected into the heavy oil reservoir through the tubing. In the tubing material selection, the gas injection pressure, temperature, and flow velocity should be considered; in the casing

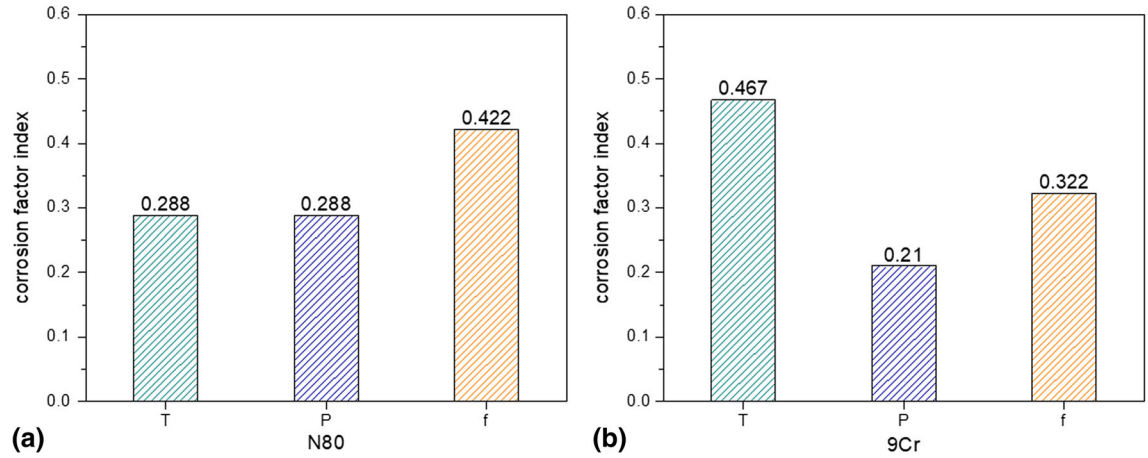

Fig. 10 Corrosion factor index of steels under different testing conditions (a: N80; b: 9Cr)

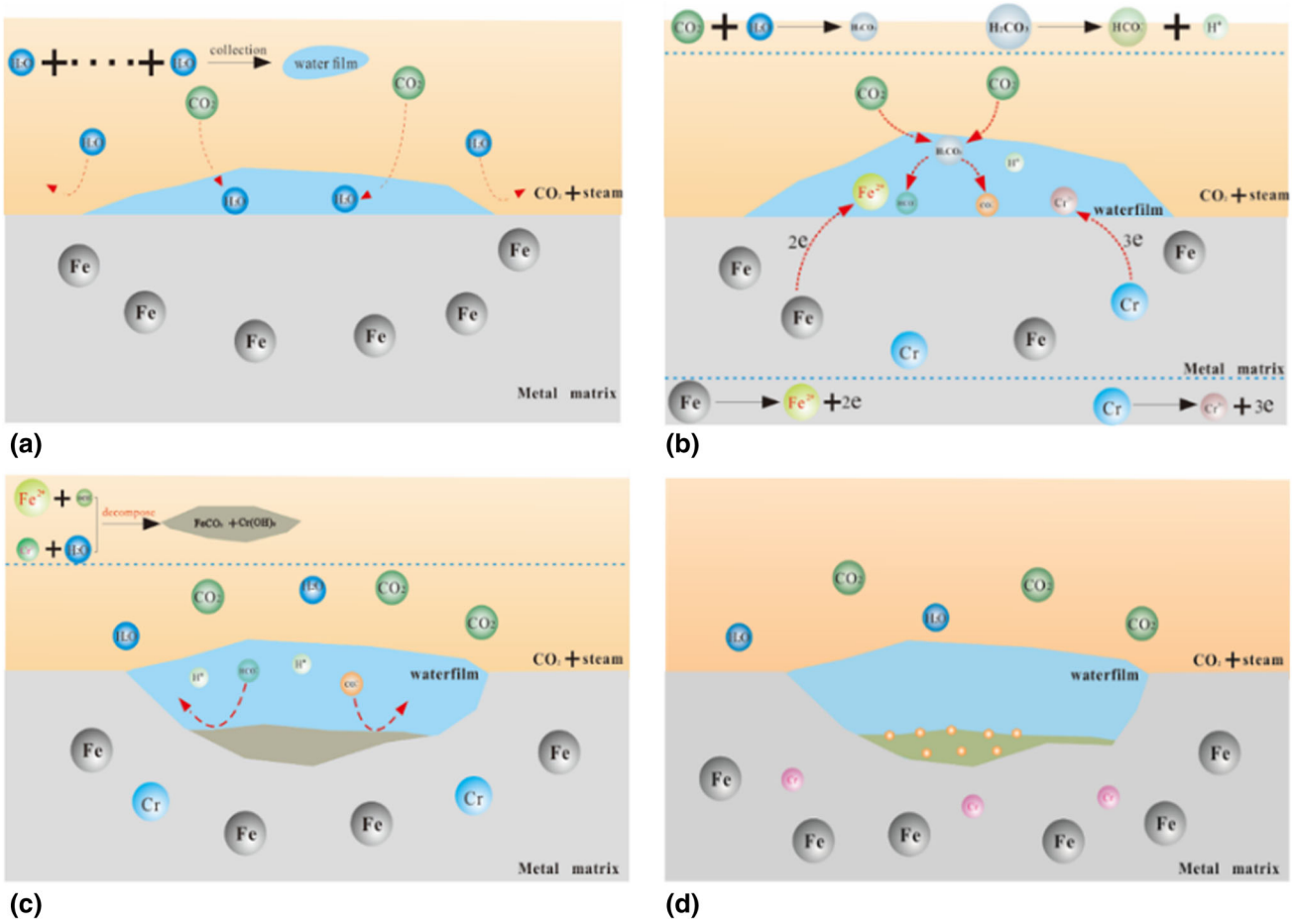

Fig. 11 Schematic diagram of the corrosion of 9Cr steel in high-temperature steam containing CO_2 (a) water-film adsorption; $_{(b)}$ anode and cathode reaction; (c) corrosion scales at low temperature; $_{(d)}$ corrosion scales at high temperature

material selection, the gas injection pressure and temperature should be considered. According to the corrosion safety factor of the material, 9Cr steel was selected as the tubing material, whereas N80 steel was selected as the casing material. Based on the corrosion impact index, the corrosion conditions of 9Cr steel were closely monitored in the high-temperature steam environment.

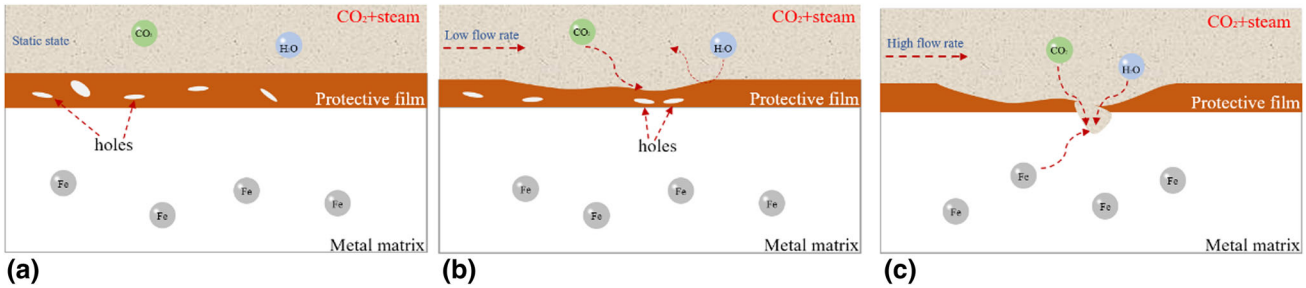

Fig. 12 Schematic diagram of the mechanism of fluid erosion corrosion scales (a: static state; b: low flow rate; c: high flow rate)

5. Conclusions

1. The corrosion resistances of 9Cr and N80 steel were compared under testing conditions. The corrosion rates of N80 and 9Cr met the application requirements in CO_2 auxiliary steam drive. The results broke the constraint of ISO-15156 standards. The flow velocity had a significant influence on the corrosion of N80 steel, and the temperature had a significant influence on the corrosion of 9Cr steel.
2. The corrosion resistance of 9Cr steel depended on the Cr-rich layer, whereas the temperature affected the amount of $FeCO_3$ on the surface and interior part of the Cr-rich layer. At the low temperature, the $FeCO_3$ content of the Cr-rich layer was relatively low. At the high temperature, the $FeCO_3$ content of the Cr-rich layer was relatively high.
3. The flow velocity affected the mass transfer process of N80 steel and the integrity of the corrosion scales. At the low flow velocity, the corrosion process was dominated by the ion diffusion process. At the high flow velocity, the corrosion process mainly depended on the integrity of the corrosion scales.
4. Considering the influence of flow velocity on the corrosion of the oil casing, 9Cr steel and N80 steel were, respectively, selected as the materials of tubing and casing in the gas injection well.

Acknowledgments

The authors acknowledge the support from National Science and Technology Major Project of China (No. 2016ZX05012-001) and the National Natural Science Foundation of China (No. 51374177).

References

1. D.W. Zhao, J. Wang, and I.D. Gates, Thermal Recovery Strategies for Thin Heavy Oil Reservoirs, *Fuel*, 2014, **117**(1), p 431–441
2. D.W. Zhao and I.D. Gates, On Hot Water Flooding Strategies for Thin Heavy Oil Reservoirs, *Fuel*, 2015, **153**, p 559–568
3. L. Xu, B. Wang, J. Zhu, W. Li, and Z. Zheng, Effect of Cr Content on the Corrosion Performance of Low-Cr Alloy Steel in a CO_2 Environment, *Appl. Surf. Sci.*, 2016, **379**, p 39–46
4. X. Lin, W. Liu, F. Wu, C. Xu, J. Dou, and M. Lu, Effect of O_2 on Corrosion of 3Cr Steel in High Temperature and High Pressure CO_2-O_2 Environment, *Appl. Surf. Sci.*, 2015, **329**, p 104–115
5. Y.S. Choi, S. Nesic, and D. Young, Effect of Impurities on the Corrosion Behavior of CO_2 Transmission Pipeline Steel in Supercritical CO_2-Water Environments, *Environ. Sci. Technol.*, 2010, **44**(23), p 9233–9238
6. L.N. Xu, S.Q. Guo, C.L. Gao, W. Chang, T.H. Chen, and M.X. Lu, Influence of Microstructure on Mechanical Properties and Corrosion Behavior of 3%Cr Steel in CO_2 Environment, *Mater. Corros.*, 2015, **63**(11), p 997–1003
7. L.M. Tavares, E.M.D. Costa, J.J.D.O. Andrade, R. Hubler, and B. Huet, Effect of Calcium Carbonate on Low Carbon Steel Corrosion Behavior in Saline CO_2 High Pressure Environments, *Appl. Surf. Sci.*, 2015, **359**, p 143–152
8. Y. Hua, R. Barker, and A. Neville, Effect of Temperature on the Critical Water Content for General and Localised Corrosion of X65 Carbon Steel in the Transport of Supercritical CO_2, *Int. J. Greenhouse Gas Control*, 2014, **31**(2), p 48–60
9. R. Elgaddafi, R. Ahmed, S. Hassani, S. Shah, and S.O. Osisanya, Corrosion of C110 Carbon Steel in High-Pressure Aqueous Environment with Mixed Hydrocarbon and CO_2 Gas, *J. Petrol. Sci. Eng.*, 2016, **146**, p 777–787
10. S.D. Zhu, A.Q. Fu, J. Miao, Z.F. Yin, G.S. Zhou, and J.F. Wei, Corrosion of N80 carbon steel in oil field formation water containing CO_2 in the absence and presence of acetic acid, *Corros. Sci.*, 2011, **53**(10), p 3156–3165
11. M. Gao, X. Pang, and K. Gao, The Growth Mechanism of CO_2 Corrosion Product Films, *Corros. Sci.*, 2011, **53**(2), p 557–568
12. Y. Zhang, X. Pang, S. Qu, X. Li, and K. Gao, Discussion of the CO_2 Corrosion Mechanism Between Low Partial Pressure and Supercritical Condition, *Corros. Sci.*, 2012, **59**(3), p 186–197
13. S. Guo, L. Xu, L. Zhang, W. Chang, and M. Lu, Corrosion of Alloy Steels Containing 2% Chromium in CO_2 Environments, *Corros. Sci.*, 2012, **63**, p 246–258
14. L. Xu, S. Guo, W. Chang, T. Chen, L. Hu, and M. Lu, Corrosion of Cr Bearing Low Alloy Pipeline Steel in CO_2 Environment at Static and Flowing Conditions, *Appl. Surf. Sci.*, 2013, **270**(4), p 395–404
15. J. Sun, C. Sun, G. Zhang, X. Li, W. Zhao, T. Jiang, H. Liu, X. Cheng, and Y. Wang, Effect of O_2 and H_2S Impurities on the Corrosion Behavior of X65 Steel in Water-Saturated Supercritical CO_2 System, *Corros. Sci.*, 2016, **107**, p 31–40
16. W. Li, L. Xu, L. Qiao, and J. Li, Effect of Free Cr Content on Corrosion Behavior of 3Cr Steels in a CO_2 Environment, *Appl. Surf. Sci.*, 2017, **425**, p 32–45
17. L. Wei, X. Pang, and K. Gao, Effect of Small Amount of H_2S on the Corrosion Behavior of Carbon Steel in the Dynamic Supercritical CO_2 Environments, *Corros. Sci.*, 2016, **103**, p 132–144
18. G.A. Zhang, D. Liu, Y.Z. Li, and X.P. Guo, Corrosion Behaviour of N80 Carbon Steel in Formation Water Under Dynamic Supercritical CO_2 Condition, *Corros. Sci.*, 2017, **120**, p 107–120
19. D. Zhu, Y. Lin, H. Zhang, Y. Li, D. Zeng, W. Liu, C. Qiang, and K. Deng, Corrosion Evaluation of Packer Rubber Materials in CO_2 Injection Wells under Supercritical Conditions, *J. Pet. Sci. Eng.*, 2017, **151**, p 311–317
20. Q.Y. Liu, L.J. Mao, and S.W. Zhou, Effects of Chloride Content on CO_2 Corrosion of Carbon Steel in Simulated Oil and Gas Well Environments, *Corros. Sci.*, 2014, **84**(84), p 165–171

21. Z.Y. Liu, X.Z. Wang, and R.K. Liu, Electrochemical and Sulfide Stress Corrosion Cracking Behaviors of Tubing Steels in a H_2S/CO_2 Annular Environment, *J. Mater. Eng. Perform.*, 2014, **23**(4), p 1279–1287
22. Y. Tang, X.P. Guo, and G.A. Zhang, Corrosion Behaviour of X65 Carbon Steel in Supercritical-CO_2 Containing H_2O and O_2 in Carbon Capture and Storage (CCS) Technology, *Corros. Sci.*, 2017, **118**, p 118–128
23. A. Pfennig and A. Kranzmann, Effect of CO_2 and Pressure on the Stability of Steels with Different Amounts of Chromium in Saline Water, *Corros. Sci.*, 2012, **65**, p 441–452
24. Q. Wu, Z. Zhang, X. Dong, and J. Yang, Corrosion Behavior of Low-Alloy Steel Containing 1% Chromium in CO_2 Environments, *Corros. Sci.*, 2013, **75**(7), p 400–408
25. G.A. Zhang and Y.F. Cheng, Localized Corrosion of Carbon Steel in a CO_2-Saturated Oilfield Formation Water, *Electrochim. Acta*, 2011, **56**(3), p 1676–1685
26. Z.F. Yin, X.Z. Wang, and L. Liu, Characterization of Corrosion Product Layers from CO_2 Corrosion of 13Cr Stainless Steel in Simulated Oilfield Solution, *J. Mater. Eng. Perform.*, 2011, **20**(7), p 1330–1335
27. Y.S. Choi, S. Nesic, and S. Ling, Effect of H_2S on the CO_2 Corrosion of Carbon Steel in Acidic Solutions, *Electrochim. Acta*, 2011, **56**(4), p 1752–1760
28. J.S. Sun, C. Sun, and X.Q. Lin, Effect of Chromium on Corrosion Behavior of P110 Steels in CO_2-H_2S Environment with High Pressure and High Temperature, *Materials*, 2016, **9**, p 200–214
29. S. Guo, L. Xu, L. Zhang, W. Chang, and M. Lu, Characterization of Corrosion Scale Formed on 3Cr Steel in CO_2-Saturated Formation Water, *Corros. Sci.*, 2016, **110**, p 123–133
30. L. Zhang, X.G. Li, and C.W. Du, Corrosion and Stress Corrosion Cracking Behavior of X70 Pipeline Steel in a CO_2-Containing Solution, *J. Mater. Eng. Perform.*, 2009, **18**(3), p 319–323
31. G.A. Zhang and Y.F. Cheng, Electrochemical Characterization and Computational Fluid Dynamics Simulation of Flow-Accelerated Corrosion of X65 Steel in a CO_2-Saturated Oilfield Formation Water, *Corros. Sci.*, 2010, **52**(8), p 2716–2724
32. G.A. Zhang, L. Zeng, H.L. Huang, and X.P. Guo, A Study of Flow Accelerated Corrosion at Elbow of Carbon Steel Pipeline by Array Electrode and Computational Fluid Dynamics Simulation, *Corros. Sci.*, 2013, **77**, p 334–341